Proceedings of 12th IOE Graduate Conference
Peer Reviewed
ISSN: 2350-8914 (Online), 2350-8906 (Print)
Year: 2022 Month: October Volume: 12

Environmental Monitoring and Modeling (EMM) of Kathmandu Valley with Remote Sensing to Understand the Drivers of Climate Change

Suyog Rai [a], Nawraj Bhattarai [b], Ram Kumar Sharma [c]

[a, c] *Department of Applied Sciences and Chemical Engineering, Pulchowk Campus, IOE, Tribhuvan University, Nepal*
[b] *Department of Mechanical and Aerospace Engineering, Pulchowk Campus, IOE, Tribhuvan University, Nepal*
[a] 076msccd015.suyog@pcampus.edu.np

Abstract
This study observes the actors of climate change by observing various environmental aspects like Normalized Difference Vegetation Index (NDVI), Land Surface Temperature (LST), Land Use Land Cover (LULC) change, Atmospheric pollutants like Aerosol Optical Depth (AOD), Methane (CH_4), Nitrogen Dioxide (NO_2), and Carbon Monoxide (CO), moreover the precipitation patterns of Kathmandu Valley. To generate the results, various Remote Sensing (RS) data were viewed and were estimated in the Google Earth Engine (GEE) code editor. The findings are according to the available data of selected sources and demonstrate that there's been a shift in the characteristics of studied parameters. There's been an increase in the NDVI value which suggests an increase in the vegetation index, however according to the LULC change results over 3 decades the forest cover declined from about 45.48% to about 37.96%. The LST in winter season have also shown an increase of 20℃ from an average of 15℃. And as the urban areas have also nearly doubled within these 3 decades, the results of the current problem with global warming are the consequences of this transition. The results of estimating the amount of pollutants in the atmosphere and precipitation levels likewise indicates increasing tendency. Between 2001 and 2021, the AOD value grew by about 30%. The CH_4 content has also increased to almost 2% in just 3 years. And the general trend for precipitation in mm/pentad is increasing, with an average increase of 28% in 2021 over 1991. Consequently, the study supports that the change in LULC like the expansion of residential areas and the addition of contaminants to the atmosphere of Kathmandu Valley are contributing to global warming.

Keywords
Climate Change, Google Earth Engine, Remote Sensing, Environmental Monitoring.

1. Introduction

The human population is continuing to congregate in the urban areas, and the intensity of human exploitation to natural resources is expanding with serious implications for biodiversity, climate and natural resources [1]. And the significant rise in air pollution emissions brought on by economic and industrial development, air quality has become a significant global environmental issue. In cities, particulate matter (PM), ozone (O_3), and nitrogen dioxide (NO_2), are the major prevalent pollutants in the air [2]. Report published in the Department of Hydrology and Meteorology (DHM) also indicates the change in precipitation cycle all over Nepal, there is declining of post-monsoonal precipitation, and the alteration of precipitation cycles over many different regions of Nepal specifies disasters such as floods, droughts, and more [3]. The study of the impacts of climate change in Nepal is thus essential as Nepalese people rely on many climate-sensitive areas. It is important to keep on monitoring the pollution levels and the environmental characteristics of a place as environment monitoring and modeling (EMM) assists in the conservation and management of natural resources, as well as human survival and progress where the changing climate puts threats to all lives. EMM is thus important in all fields, as a part of environmental research scientists require monitoring, moreover to plan and evaluate effective environmental policies, policymakers also require monitoring [4]. There are various methods in monitoring pollution

levels and other drivers of climate change, where the technique like RS makes it possible to monitor spatial and temporal characteristics of a place quickly and affordably [5]. Using satellite-based RS technology, the quality of the air over a long period and at different scales can be monitored. Moreover, the changes in the spatial characteristics of a place can be noticed. Accordingly with the help of RS data such as Landsat, Sentinel, CHIRPS and MODIS various environmental parameters of the region of interest (ROI) have been classified and estimated in Google Earth Engine (GEE) and later the maps obtained are displayed with the help of ArcGIS (Geographic Information System) software. The study area is described in section 3, and the suggested approaches and retrieval procedures for EMM of ROI are presented in Section 4. Results and Discussion are shown in Sections 5 and 6, respectively. And lastly, the conclusion is given in Section 7.

2. Research Objectives

The main objective of the study is to view the changes in the environmental parameters of Kathmandu valley in the past years with RS techniques. And the specific objectives include: i. Land Use Land Cover (LULC) change progress monitoring ii. Observing the green space and land surface heat iii. Estimating the atmospheric pollution levels and Precipitation patterns

3. Study Area

The study area for this project is Kathmandu Valley, the central region of Nepal covering a total area of approximately 954 square kilometers. The valley is confined in 27°47'9.68"N and 85°24'14.23"E in the north, 27°39'32.48"N and 85°28'10.47"E in the east, 27°41'8.32"N and 85°13'2.75"E in the west, and 27°27'48.11"N and 85°20'25.26"E in the south. The valley's largely level floor is 1300 meters above sea level, while its steeply sloping slopes reach altitudes of more than 2000 meters [6]. Kathmandu valley comprises the most populated cities of Nepal with unplanned urbanization, and these cities are also responsible for global warming.

4. Materials and Methods

The first step for every process is to review the satellite imagery. In this study, environmental parameters were retrieved from RS data such as Landsat satellite data, Sentinel, and MODIS. Since 2015, Sentinel-2 was built and run by European Space Agency (ESA) and has been transmitting data for land monitoring, emergency responses, and security services [7]. While, the Landsat satellite series is the longest record of observation of the Earth from space [8], so landsat 5 Thematic Mapper (TM) and Landsat 8 Operational Land Imager and Thermal Infrared Sensor (OLI/TIRS) including Sentinel data and others as desired were used in the process.

4.1 Normalized Difference Vegetation Index (NDVI)

Vegetation indices are useful and empirical indicators that indicate the level of vegetation and characterize ecological conditions [1]. Normalized Difference Vegetation Index (NDVI) is one of the indices, where the index ranges from -1 to 1, of which the negative values indicate snow cover, water body and clouds, and the positive values display the bare land and more vegetation [9]. The growth of NDVI through time was examined using the Landsat 5 and 8 images and the GEE tool. Landsat 5 TM Collection 1 Tier 1 calibrated top-of-atmosphere (TOA) reflectance from 1991 to 2011 and then Landsat 8 Collection 1 Tier 1 calibrated top-of-atmosphere (TOA) reflectance to 2021 datasets were used for evaluating the NDVI of ROI.

4.2 Land Surface Temperature (LST)

There are various ways by which the LST of respective ROI can be determined either by using the Landsat satellite images or MODIS imagery.

4.2.1 Landsat LST

The United States Geological Survey (USGS) provides TOA brightness temperatures for the Landsat thermal infrared (TIR) channels, which are completely accessible and ready to use in GEE for Landsats 4–8, collection 1 [10]. All of the findings in this study or the data used in the code are supported by Tier 1 data.

4.2.2 Moderate Resolution Imaging Spectroradiometer (MODIS) LST

The MOD11A2 Version 6 product provides an average 8-day per-pixel Land Surface Temperature and Emissivity (LST&E) with a 1 kilometer (km) spatial resolution in a 1200 by 1200 km grid [11]. The

data for MODIS land products have been available since 2000; hence for the analysis of LST of ROI the date range is from the availability of the data set period to 2022-06-30. The MOD11A2 product's current algorithm uses the simple average technique [12].

4.3 Land Use Land Cover (LULC) Classification

Changes in LULC have been explored using multi-temporal Landsat Thematic Mapper/Enhanced Thematic Mapper Plus/Operational Land Imager (TM/ETM+/OLI) images [13, 14]. The land classes used in this study is presented by Table (1), WaterBody, Urban, Forest, Cropland and Bareland are the five land classes used in this study.

Table 1: Land class types descriptions.

Land Class	Training Symbol	Description
WaterBody	0	Lakes, Ponds and Rivers
Urban	1	Residential Areas
Forest	2	Trees, Forest and Forestry
CropLand	3	Agricultural Land
BarrenLand	4	Shrubland, Grassland, Barren soils

4.4 Atmospheric Pollution Concentration

4.4.1 Aerosol Optical Depth (AOD)

AOD is a wavelength-dependent indicator of the number of aerosols in the atmosphere; high AOD values suggest a generally foggy environment, while low AOD values indicate a generally clear atmosphere [15]. The AOD is monitored every day by NASA's Terra satellite's MODIS sensors. In this study, an investigation or the study of MODIS-derived AOD from 2001 to 2021 (two decades) was made using Google Earth Engine (GEE). For the aerosol algorithms in the analysis, MCD19A2 Version 6 data products were employed. The MCD19A2 Version 6 data product is a daily, 1-km-resolution, combined MODIS Terra and Aqua Multi-angle Implementation of Atmospheric Correction (MAIAC) Land Aerosol Optical Depth (AOD) gridded Level 2 product [16].

4.4.2 Methane (CH_4)

To calculate CH4 emissions at a global or regional scale, TROPOMI is one of the quick and easy methods. Compared to other CH4 measuring instruments, the TROPOMI on board the Sentinel 5 Precursor (S5-P) satellite has measured CH4 with an unprecedented resolution of 7×7 km2 [17]. Hence, the study evaluates the performance of Sentinel 5-P OFFL CH4: Offline Methane for monitoring the methane (CH4) concentration of study area. Methane averaged mixing ratio in dry air, as measured by columns in parts-per-billion-volume (ppbV) is observed by CH4 column volume mixin ratio dry air band from the starting date of the dataset availability 2019-02-08 to 2022-06-30.

4.4.3 Nitrogen Dioxide (NO_2)

Sentinel-5P NRTI NO2: Near Real-Time Nitrogen Dioxide data was used to understand the NO2 of study region which is provided by TROPOMI that employs passive remote sensing methods by measuring the solar radiation that the Earth reflects and radiates at the TOA [18]. NO2 column number density band which is the total NO2 vertical column (ratio of the slant column density of NO2 and the total air mass factor) of unit mol/m$\hat{2}$ was used from Sentinel-5P NRTI NO2: Near Real-Time Nitrogen Dioxide and the results are displayed by the following figures. The dataset availability is from 2018-07-10 hence only three years from 2019 to 2021 have been analysed.

4.4.4 Carbon Monoxide (CO)

Another major pollutant in the urban area is Carbon Monoxide (CO). To monitor the CO worldwide the Sentinel 5 Precursor (S5P) satellite's TROPOMI instrument takes Earth radiance measurements in the 2.3 μm spectral range of the shortwave infrared (SWIR) region of the sun spectrum [19]. The result shows the TROPOMI CO observations on study area by using CO column number density band of Sentinel-5P NRTI CO: Near Real-Time Carbon Monoxide. The study was conducted from 2018-11-22 to 2022-05-30; however, as our primary goal was to track the CO concentration during the whole year, only three years 2019, 2021, and 2022 that had complete data were examined for the findings and discussion

4.5 Precipitation

Since, 1981 the rainfall data sets are provided by the Climate Hazards Group InfraRed Precipitation with Station Data (CHIRPS) [20]. The database has a spatial resolution of 0.05°×0.05°, and quasi-global coverage (50°N - 50°S, 180°W - 180°E) which is the high-resolution of the data that is provided as compared to other existing off-site precipitation database [21]. Hence, it is also important to

understand the precipitation/rainfall patterns of a region to understand the impacts of climate change. So, the precipitation pattern of the study site was noticed using CHIRPS with the help of GEE.

5. Results

5.1 Normalized Difference Vegetation Index (NDVI)

The NDVI was computed in GEE using Landsat satellites data collected over more than three decades, from 1988 to 2021. The obtained results were analyzed by taking both the images containing cloud cover and by removing the clouds (cloud mask) in the images. The figure (1) and (2) shows the growth of NDVI values from 1988 to 2021. Figure (1) shows the NDVI values for images (satellite data) with clouds over ROI, but our major interest is in the values obtained for images without clouds, so we mainly focus on the values in Figure (2). However, both the figures display the increasing trendline of NDVI indicating the rise in the vegetation cover. Figure (2) shows that the NDVI value was 0.326 at the start of the research year and increased to 0.492 by 2021. Similar observations can be seen in figure (1), where the value rose from 0.3045 to 0.418. As a result, despite all the changes throughout the years, the NDVI is showing a continuous increasing line.

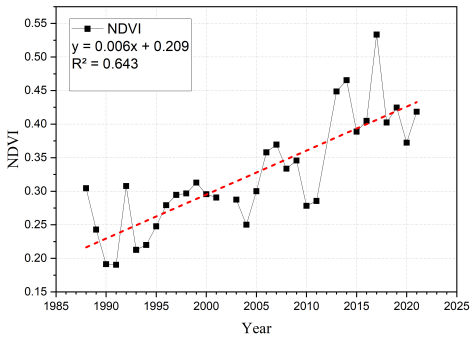

Figure 1: Average NDVI of a year (With Clouds) since 1988 to 2021

5.2 Land Surface Temperature (LST)

5.2.1 Landsat LST

LST estimation procedure was executed using Landsat 5, 7 and 8 satellite data in GEE, and the results are presented in the following figure (3) that illustrates the land temperature in degree Celsius of four seasons.

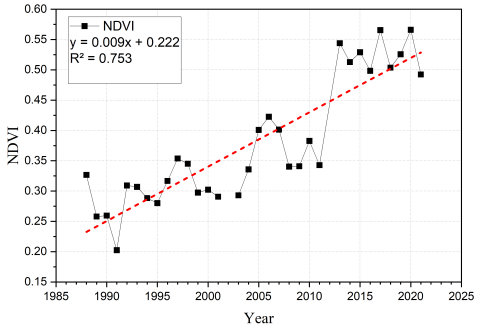

Figure 2: Average NDVI of a year (Cloud Masked) since 1988 to 2021

5.2.2 MODIS LST

Likewise, the result obtained by using MOD11A2 of C6 MODIS LST in degree Celsius is illustrated in figure (4) from 2000 to 2021.The trendline once more demonstrates the decline in the average LST like the results obtained from Landsat satellites. Nevertheless, they are only the typical LST for the whole Kathmandu Valley. Now, after viewing the areas that contained specific LST values, the findings are shown in Figure (5). The LST values were divided into four classes 14°C - 18°C, 18.01°C - 22°C, 22.01°C - 26°C and 26.01°C - 28°C and above. Now from figure (5), it can be noticed that areas that had LST values in the range of 18.01°C - 22°C are rising followed by slight increment of 26.01°C - 28°C values while the areas with 14°C - 18°C are almost neutral. Only the regions with values between 22.01°C - 26°C are seeing a declining trendline. However, when the results between 2000 and 2021 are examined, it is estimated that 59% of the whole Kathmandu Valley had LST in the range between 22.01°C - 26°C in 2000, which decreased to 51% by 2021. While the area grew from 6% to 7% with 14°C - 18°C and it climbed from 24% to 33% with 18.01°C - 22°C. But for 26.01°C - 28°C, the area increment or decrement varied considerably, starting at 9% in 2000, climbing to 18% in 2018, then falling down to 7% by 2021 making it a nearly straight trendline.

5.3 Land Use Land Cover (LULC) Change

After performing the Random Forest (RF) Classification analysis, the results and maps are here as depicted table (2) and figure (6). It can be seen from this table that the residential areas are growing by looking at the Urban Land Class data. The urban class delineated about 10.49% (97.93 km^2) of the total

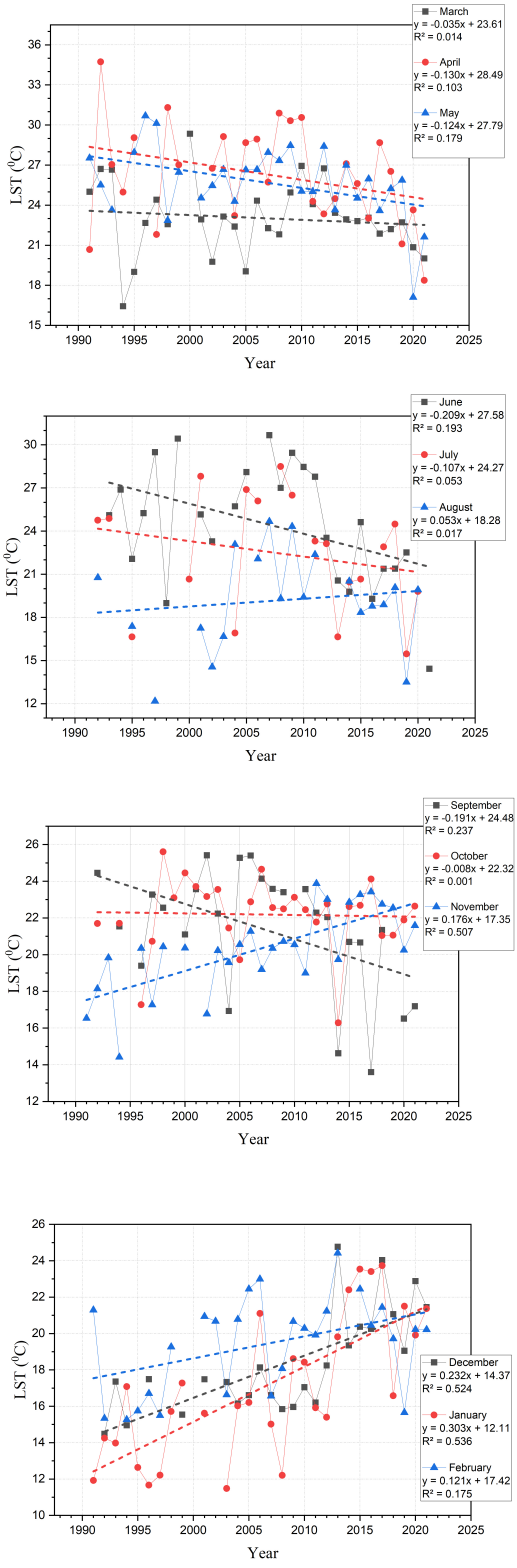

Figure 3: LST of Kathmandu Valley by averaging the data recorded by Landsat 5, 7 and 8 satellites in four different seasons)

area of Kathmandu Valley in 1991, which reached to about 22.26% (207.82 Km^2) in 2021. The data as a

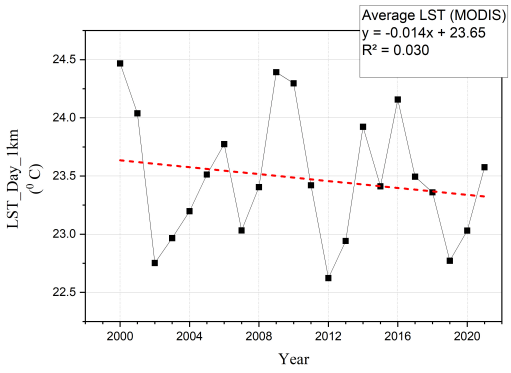

Figure 4: Averaged LST of Kathmandu Valley in two decades using MODIS data

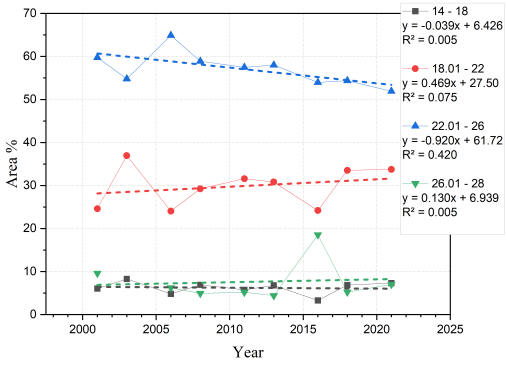

Figure 5: Percentage (%) of Kathmandu Valley Area Occupying Certain LST

whole shows an upward trend. Besides about 45.48% (424.57 Km^2) of the area was occupied by forest class, 27.55% (257.15 Km^2) by cropland, and about 16.46% (153.63 Km^2) by barrenland in the year 1991. This has now turned to about 37.96% (354.39 Km^2) by forest class, 27.90% (260.46 Km^2) by cropland, and about 11.80% (110.14 Km^2) by barrenland in 2021. Here, aside from the clear observation with residential areas, the forest, cropland and barrenland features may have the possibility of getting mixed. Because of this difficulty in separating the features during classification, there are slight to moderate fluctuations over these land classes, nevertheless the trend line is assuming a little increase throughout the years. Also, with water body class there may have been difficulty in classifying its features as the water bodies occupy minor surface areas of Kathmandu Valley compared to other land classes. As a consequence, although the data for this waterbody class has been obtained its trendline is neglected for observation.

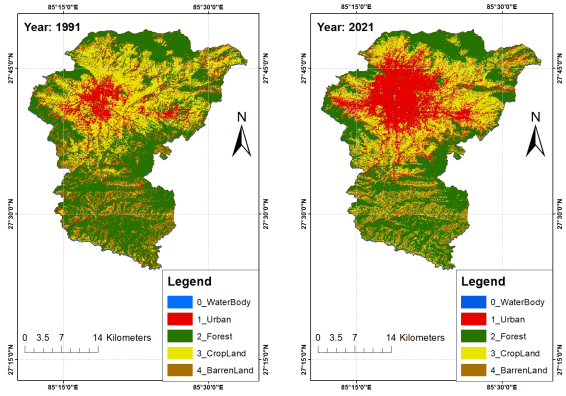

Figure 6: LULC maps of Kathmandu valley in respective in 1991 and 2021

Table 2: Area in Square Kilometers and percentage of the Kathmandu valley of studied land classes as obtained by the classification process in GEE in respective study years

Year	WaterBody Area (%)	Urban Area (%)	Forest Area (%)	Cropland Area (%)	Barrenland Area (%)
1991	0.03	10.49	45.48	27.55	16.46
1996	0.04	16.07	45.17	32.25	6.47
2001	0.02	18.97	43.40	17.60	20.00
2011	0.01	19.27	42.96	20.74	17.02
2016	0.11	21.20	52.59	17.67	8.42
2021	0.08	22.26	37.96	27.90	11.80

5.4 Atmospheric Pollution Concentration

5.4.1 Aerosol Optical Depth (AOD)

Figure (7) shows the AOD that was produced using the Optical Depth 047 band in GEE for 20 years from 2001 to 2021. The AOD values are given on a scale from 0.001 to 1, where rating of 0.4 suggests hazy air conditions, a number or value of 0.01 indicates an exceedingly clean atmosphere, and AOD greater than 1 denotes extreme air pollution conditions [22]. The data show that in 2001, the AOD value was 0.358, and then it climbed gradually until it reached 0.472 in 2016. The values decreased again but were still higher than 2001 levels, and later reached 0.489, the highest in twenty years. The overall AOD value is likewise trending upward.

5.4.2 Methane (CH_4)

Column averaged dry mixing ratio of Methane (CH4) in parts per billion volumes (ppbV) of Kathmandu valley is illustrated by the figure (8) for January, February and March months and figure (9) for October, November and December months. Since, other than these selected months there was negligible to no data taken by the satellite as estimated in GEE.

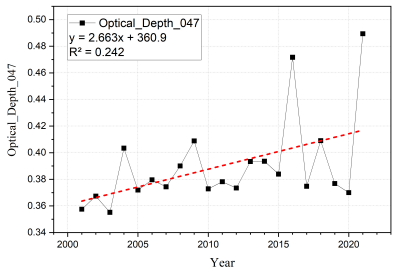

Figure 7: Aerosol Optical Depth (AOD) of Kathmandu Valley over two decades using band Optical Depth 047

The data was collected from January through March over four years, and it is now clear that in 2019, the CH_4 value at the start of the study year was around 1854.08 ppbV, and then it reached to 1886.07 ppbV in 2022. Likewise, just three years were examined for October through December. The value of CH_4 was 1876.868 ppbV in 2019 and increased to 1914.296 ppbV in 2021. This entire body of data demonstrates the rise in atmospheric CH4 concentration over the ROI.

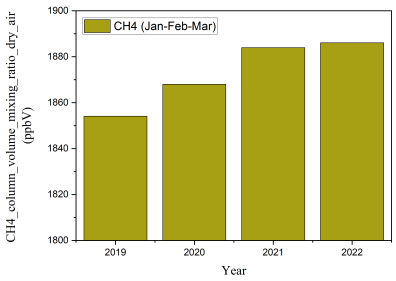

Figure 8: Column averaged dry air mixing ratio of methane in ppbV from 2019 to 2022 in January, February and March months

5.4.3 Nitrogen Dioxide (NO_2)

The starting date for NO_2 is available from July 2018 hence for time series that covers three whole years average data are from 2019 to 2021 only which is presented in figure (10). NO_2 in mole per meter square (mol/m2) in 2019 was about 0.00006924, followed by 0.00006386 in 2020 and 0.00007044 in 2021. The value decreased in the year 2020 and again took a great jump. Once more, the data shows a decrease in 2020 that abruptly increased in 2021.

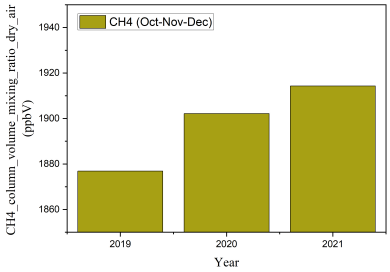

Figure 9: Column averaged dry air mixing ratio of methane in ppbV from 2019 to 2021 in October, November and December months.

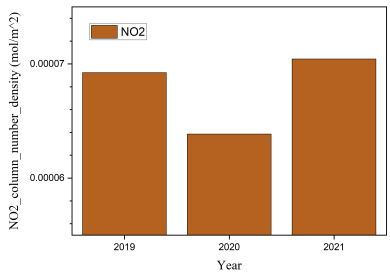

Figure 10: Total vertical column (Tropospheric and Stratospheric) Nitrogen Dioxide (NO2) concentration of Kathmandu valley from 2019 to 2021

5.4.4 Carbon Monoxide (CO)

Similar to CH_4 and NO_2, CO's TROPOMI data are only recently available, therefore only three years beginning in 2019 have been examined. The CO content in the air above the Kathmandu Valley was 0.0340 mol/m2 in 2019, 0.0336 mol/m2 in 2020, and then a sharp increase to 0.0363 mol/m2 in 2021 as depicted by the figure (11). Likewise to the other investigated pollutants, CO is on the rise.

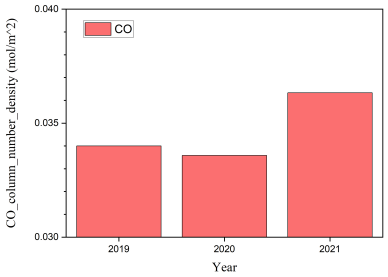

Figure 11: CO concentration of Kathmandu Valley in mol/m2 from 2019 to 2021

5.5 Precipitation

The data from CHIRPS was extracted and estimated in GEE and the results were obtained. The figure (12) indicates the average precipitation in each year of Kathmandu valley over three decades. Although there have been numerous swings throughout the years, from roughly 17.78 mm/pentad in 1991 to 24.60 mm/pentad in 2002, and again dropping to 16.42 mm/pentad in 2005, it is obvious from this data that precipitation is increasing which has reached to 24.83 mm/pentad in 2021.

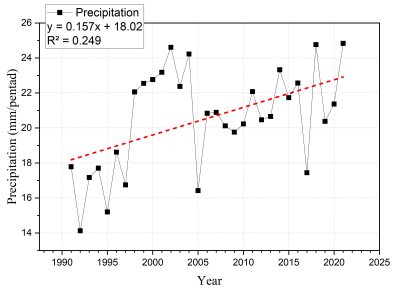

Figure 12: Average Precipitation of Kathmandu Valley in mm/pentad over three decades from 1991 to 2021 using CHIRPS product.

6. Discussion

Despite many fluctuations, the results indicated either an increasing or decreasing trendline of studied parameters. Here for satellite images with clouds and with clouds masked, the obtained NDVI values at the beginning of the research year 1998 were 0.30, but at the conclusion of the study year 2021, the values were 0.41 and 0.49. Although it doesn't specifically show an increase in forests or trees, this does imply that the vegetation cover has increased either in grassland or cropland. While looking as the data for LULC the forest land cover (table (2)) has declined from about 45.48% to 37.96%. In this case, the NDVI time series investigation does not clearly demonstrate the source of global warming. So, in order to identify the causes of climate change, we look at other factors. When viewing the LST results, particularly focusing on the average value of all three landsat satellites (L5, L7 and L8), winter season LST is inclining rapidly. LST in this season has increased to levels of 20°C from an average of 15°C at the start of the observed years. These consequences of an increase in the average surface temperature include serious issues like global

warming. On the contrary, the LST for the rest of the seasons is in the opposite trend, which has also been depicted by the data derived from MODIS LST results. On dividing the LST values into four groups (14°C - 18°C, 18.01°C - 22°C, 22.01°C - 26°C and 26.01°C - 28°C) as illustrated by figure (5), it has now been clear that that areas with temperature classes of 14°C - 18°C and 18.01°C - 22°C, and 22.01°C - 26°C and 26.01°C - 28°C are rising and falling, respectively. The implications of this transition are the results of the present issues with global warming. Even as seen from the LULC for Urban class, which has been expanding tremendously that nearly doubled from 1991 level. Rapid urbanization is thus changing the biophysical environment by having a significant influence on many facets of our life including all the lives in that location. Likewise, the findings of evaluating the quantity of contaminants in the atmosphere, another crucial criterion for comprehending the causes of climate change, are frightening. In practically every pollutants that was measured, an increasing trend could be seen. Starting from the AOD results, which were examined over a 20 years, a growing movement was detected. The AOD value has increased by around 30% between 2001 and 2021. This atmospheric aerosol particles explicitly impact the incoming solar energy, which also alters cloud characteristics resulting in a result it is one of the gasp associated with predicting climate uncertainty [23]. Even so the AOD is escalating the 2020 experienced the lowest AOD value 0.37 of the decade (from 2010 to 2021). Similar outcomes were found for NO_2, where the 2020 data sharply decreased. The air pollution levels depletion this year is mainly as a result of the Coronavirus (Covid-19) pandemic and the subsequent closure of public spaces. Many reports have also indicated the reductions in NO2, HCHO, SO_2, CO, and AOD during this period over East Asia [24]. This is all the reflection of the operations employing fossil fuels and other activities that were being shut down. Correspondingly, the estimated data of CO also dropped in 2020 and suddenly rose to about 6% after the lockdown in Kathmandu valley. But ever since the observation date, the CH_4 concentration has been steadily increasing. Within the last few years, the atmospheric concentration of CH_4 has climbed to roughly 2%. And lastly, after reviewing the outcomes of precipitation pattern over 30 years, we observed the changes that had happened. The overall trend of precipitation in mm/pentad is clearly rising with an average of 28% rise in 2021 as compared to 1991. From the outcomes of EMM of the study area, it is clear about the change in the physical aspects that are happening over these years. Urban land is enlarging, leading to the urbanization induced global warming. Urbanization alters the surface climate in urban areas by affecting the local land surface [25],and as our calculations indicate GHG emissions will continue to increase sharply unless we could learn from the lockdown from Covid-19, when most of life's comforts were switched off.

7. Conclusions

Environmental monitoring and modelling of a location are required to comprehend the causes of climate change where remote sensing is one of the simplest and quickest methods. And based on the desired parameter, appropriate data from various remote sensing devices were employed and estimated in GEE. This study supports Kathmandu Valley's contribution to global warming by demonstrating the expansion of residential areas and the accession of pollutants like AOD, CH4, NO2, and CO to the region's atmosphere. The study has also observed the changes in the range of environmental parameters from the increment of overall NDVI values to the decrement of average LST. Understanding the various factors and how they interact can therefore assist to understand the causes of climate change. Even though some of the observed data only covered a short period, their levels have undergone an unheard-of growth, and this increase in pollution will undoubtedly affect our planet's climate. As a consequence, this project will provide experts an invaluable chance to learn more about the factors that contribute to climate change. We may assess the existing conditions of environmental systems via using remote sensing monitoring programs, which further emphasizes the overall need for conservation and management efforts. Perhaps one of the greatest issues that should be addressed using remotely sensed data approaches in the future and present now is climate change.

Acknowledgments

The author gratefully acknowledges the assistance provided by Professors and staffs of Department of Applied Sciences and Chemical Engineering and Pulchwok Campus, IOE for their direction, inspiration, and ongoing support throughout this

project. Also deserving of praise are the university's librarians, research assistants, and study participants who had an influence in this project.

References

[1] Jun Li, Yanqiu Pei, Shaohua Zhao, Rulin Xiao, Xiao Sang, and Chengye Zhang. A review of remote sensing for environmental monitoring in china. *Remote Sensing*, 12(7), 2020.

[2] Gennaro D'Amato, L Cecchi, M D'amato, G Liccardi, et al. Urban air pollution and climate change as environmental risk factors of respiratory allergy: an update. *Journal of Investigational Allergology and Clinical Immunology*, 20(2):95–102, 2010.

[3] R Karki. Hasson s ul, schickhoff u, scholten t, böhner j. 2017. rising precipitation extremes across nepal. climate, 5 (1): 4.

[4] John W Williams and Stephen T Jackson. Novel climates, no-analog communities, and ecological surprises. *Frontiers in Ecology and the Environment*, 5(9):475–482, 2007.

[5] Katherine S Willis. Remote sensing change detection for ecological monitoring in united states protected areas. *Biological Conservation*, 182:233–242, 2015.

[6] Barry N Haack and Ann Rafter. Urban growth analysis and modeling in the kathmandu valley, nepal. *Habitat International*, 30(4):1056–1065, 2006.

[7] Matthias Drusch, Umberto Del Bello, Sébastien Carlier, Olivier Colin, Veronica Fernandez, Ferran Gascon, Bianca Hoersch, Claudia Isola, Paolo Laberinti, Philippe Martimort, et al. Sentinel-2: Esa's optical high-resolution mission for gmes operational services. *Remote sensing of Environment*, 120:25–36, 2012.

[8] Charlie J Tomlinson, Lee Chapman, John E Thornes, and Christopher Baker. Remote sensing land surface temperature for meteorology and climatology: A review. *Meteorological Applications*, 18(3):296–306, 2011.

[9] Asmala Ahmad and Shaun Quegan. Comparative analysis of supervised and unsupervised classification on multispectral data. *Applied Mathematical Sciences*, 7(74):3681–3694, 2013.

[10] Sofia L Ermida, Patrícia Soares, Vasco Mantas, Frank-M Göttsche, and Isabel F Trigo. Google earth engine open-source code for land surface temperature estimation from the landsat series. *Remote Sensing*, 12(9):1471, 2020.

[11] Mod11a2 v006. `https://lpdaac.usgs.gov/products/mod11a2v006/`.

[12] Zhengming Wan. Collection-5 modis land surface temperature products users' guide. *ICESS, University of California, Santa Barbara*, 2007.

[13] Peng Dou and Yangbo Chen. Dynamic monitoring of land-use/land-cover change and urban expansion in shenzhen using landsat imagery from 1988 to 2015. *International Journal of Remote Sensing*, 38(19):5388–5407, 2017.

[14] M Rafiqul Islam, M Giashuddin Miah, and Yoshio Inoue. Analysis of land use and land cover changes in the coastal area of bangladesh using landsat imagery. *Land Degradation & Development*, 27(4):899–909, 2016.

[15] Marios Theristis, Venizelos Venizelou, George Makrides, and George E Georghiou. Energy yield in photovoltaic systems. In *McEvoy's handbook of photovoltaics*, pages 671–713. Elsevier, 2018.

[16] Mcd19a2.006: Terra & aqua maiac land aerosol optical depth daily 1km. `https://developers.google.com/earth-engine/datasets/catalog/MODIS_006_MCD19A2_GRANULES`.

[17] Mengyao Liu, Ronald van der A, Michiel van Weele, Henk Eskes, Xiao Lu, Pepijn Veefkind, Jos de Laat, Hao Kong, Jingxu Wang, Jiyunting Sun, et al. A new divergence method to quantify methane emissions using observations of sentinel-5p tropomi. *Geophysical Research Letters*, 48(18):e2021GL094151, 2021.

[18] Sentinel-5p tropomi user guide. `https://sentinel.esa.int/web/sentinel/user-guides/sentinel-5p-tropomi`.

[19] O Hasekamp, A Lorente, H Hu, A Butz, J de Brugh, and J Landgraf. Algorithm theoretical baseline document for sentinel-5 precursor methane retrieval. *Netherlands Institute for Space Research*, page 67, 2019.

[20] D Auliyani and N Wahyuningrum. Rainfall variability based on the climate hazards group infrared precipitation with station data (chirps) in lesti watershed, java island, indonesia. In *IOP Conference Series: Earth and Environmental Science*, volume 874, page 012003. IOP Publishing, 2021.

[21] Dimitrios Katsanos, Adrianos Retalis, and Silas Michaelides. Validation of a high-resolution precipitation database (chirps) over cyprus for a 30-year period. *Atmospheric Research*, 169:459–464, 2016.

[22] Esrl global monitoring laboratory - global radiation and aerosols. `https://gml.noaa.gov/grad/surfrad/aod/`.

[23] Mikhail D Alexandrov, Igor V Geogdzhayev, Kostas Tsigaridis, Alexander Marshak, Robert Levy, and Brian Cairns. New statistical model for variability of aerosol optical thickness: Theory and application to modis data over ocean. *Journal of the atmospheric sciences*, 73(2):821–837, 2016.

[24] Masoud Ghahremanloo, Yannic Lops, Yunsoo Choi, and Seyedali Mousavinezhad. Impact of the covid-19 outbreak on air pollution levels in east asia. *Science of the Total Environment*, 754:142226, 2021.

[25] Huimin Liu, Bo Huang, and Chen Yang. Assessing the coordination between economic growth and urban climate change in china from 2000 to 2015. *Science of the total environment*, 732:139283, 2020.